nature
cell biology

The ubiquitin ligase CHIP acts as an upstream regulator of oncogenic pathways

Masashi Kajiro[1,6], Ryuichi Hirota[1,6], Yuka Nakajima[1], Kaori Kawanowa[2], Kae So-ma[1], Ichiaki Ito[1], Yuri Yamaguchi[3], Sho-hei Ohie[1], Yasuhito Kobayashi[2], Yuko Seino[3], Miwako Kawano[1], Yoh-ichi Kawabe[1], Hiroyuki Takei[2], Shin-ichi Hayashi[4], Masafumi Kurosumi[2], Akiko Murayama[1,5], Keiji Kimura[1] and Junn Yanagisawa[1,5,7]

CHIP is a U-box-type ubiquitin ligase that induces ubiquitylation and degradation of its substrates, which include several oncogenic proteins[1–12]. The relationship between CHIP and tumour progression, however, has not been elucidated. Here, we show that CHIP suppresses tumour progression in human breast cancer by inhibiting oncogenic pathways. CHIP levels were negatively correlated with the malignancy of human breast tumour tissues. In a nude mouse xenograft model, tumour growth and metastasis were significantly inhibited by CHIP expression. In contrast, knockdown of *CHIP* (sh*CHIP*) in breast cancer cells resulted in rapid tumour growth and metastatic phenotypes in mice. In cell-based experiments, anchorage-independent growth and invasiveness of sh*CHIP* cells was significantly elevated due to increased expression of *Bcl2*, *Akt1*, *Smad* and *Twist*. Proteomic analysis identified the transcriptional co-activator SRC-3 (refs13–19) as a direct target for ubiquitylation and degradation by CHIP. Knocking down *SRC-3* in sh*CHIP* cells reduced the expression of *Smad* and *Twist*, and suppressed tumour metastasis *in vivo*. Conversely, SRC-3 co-expression prevented CHIP-induced suppression of metastasis formation. These observations demonstrate that CHIP inhibits anchorage-independent cell growth and metastatic potential by degrading oncogenic proteins including SRC-3.

We examined the mRNA and protein levels of CHIP (carboxyl terminus of Hsc70-interacting protein) in human breast cancer tissues, as it controls protein levels of several oncogenic proteins[9–12], including oestrogen receptor α (ERα). Samples of breast cancer tumours and normal tissue were obtained from 27 patients with breast cancer (Supplementary Information, Table S1), and the expression levels of *CHIP* mRNA were examined. In cancerous tissues from patients clinically determined to be stage I (Fig. 1a), or from node-negative patients (Fig. 1b), we found that the level of *CHIP* mRNA expression was comparable to that observed in the corresponding normal breast tissue ($P = 0.83$, Fig. 1a and $P = 0.16$, Fig. 1b). Tumours from stage II patients (Fig. 1a) or those from node-positive (N1a) patients (Fig. 1b) showed decreased levels of *CHIP* mRNA, compared with the non-cancerous tissues ($P < 0.001$, Fig. 1a, b). These results demonstrate a significant negative correlation between *CHIP* mRNA levels and tumour malignancy in human breast cancer tissues. We also compared the correlation between *CHIP* mRNA levels and tumour grade using the Oncomine database, which provides publicly available cancer gene expression datasets. Nine of 21 datasets that contain gene chip profiles classified by breast tumour grade, showed an inverse correlation between *CHIP* mRNA expression and tumour grade, consistent with our results. Two datasets characterized by large population sizes showed a significant inverse correlation between *CHIP* expression levels and tumour grade (Desmedt_Breast and vantVeer_Breast, $P = 0.00035$ and $P = 0.00093$, respectively). Immunohistochemical staining indicates that expression levels of CHIP proteins also decreased in malignant tumours (Fig. 1c). Thus, these results demonstrate that CHIP protein and mRNA levels were reduced in the invasive tumour region. As CHIP is a ubiquitin ligase for ERα, we expected the inverse correlation between *CHIP* mRNA and ERα protein levels. We did not observe a significant correlation between *CHIP* expression and ERα positivity ($P = 0.18$; Fig. 1d). Moreover, none of the 32 datasets from the Oncomine database (each dataset contains gene chip profiles classified by ERα positivity) demonstrated an inverse correlation between *CHIP* expression levels and ERα positivity.

We then examined whether tumour progression was enhanced when the expression level of CHIP was downregulated. Protein levels of CHIP were much higher in MCF-7 cells, a non-aggressive cell line derived from human breast cancer cells, than in MDA-MB-231 cells, a highly aggressive cell line (Fig. 2a). We generated three MCF-7 clones in which endogenous *CHIP* expression was knocked down by a short hairpin RNA (shRNA; Fig. 2b). To investigate the effects of *CHIP* knockdown *in vivo*, ten nude

Figure 1 Decreased CHIP expression in malignant breast tumour tissues. (**a**, **b**) *CHIP* mRNA expression in breast tumours. Total RNA was prepared from normal (N) or tumour (T) tissues and the *CHIP* mRNA level was quantified using real-time RT–PCRs. Total RNA was prepared from tissues of stage I and stage II patients (**a**) or from node-negative (N0) and node-positive (N1a) patients (**b**). The cut-off points were determined using ROC (receiver operating characteristics) curve-based statistical analysis. Statistical significance of the differences between the groups was determined by *t*-test.

Open circles, CHIP-positive; filled circles, CHIP-negative. (**c**) Representative images of immunohistochemical labelling of CHIP and haematoxylin and eosin (H&E) staining. The tumour tissues were derived from stage II or N1a patients (tissue samples nos 1–3). Normal (N) or tumour (T) tissues are marked with dotted lines. Scale bars, 100 μm. (**d**) Relationship between *ERα* and *CHIP* mRNA expression in breast tumours. Total RNA was prepared from *ERα*-positive or *ERα*-negative tumour tissues and the *CHIP* mRNA level was quantified using real-time RT–PCRs.

mice received bilateral subcutaneous flank injections of sh*CHIP* MCF-7 cells or control cells. The tumours in three groups that were injected with sh*CHIP* cells increased in size, whereas little tumour growth was observed in mice injected with control cells (Fig. 2c, d). Histological examination revealed that, compared with control cells, the sh*CHIP* tumour cells had a higher degree of nuclear atypia and a higher mitotic index (Fig. 2e). In addition, immunostaining of α-smooth muscle actin (SMA) demonstrated that the density of vessels in the tumours was higher in the sh*CHIP* tumours than in control tumours (Fig. 2f).

To further confirm the suppressive function of CHIP in tumour progression, we generated MDA-MB-231 cells that overexpressed CHIP (CHIP^OE^; Fig. 2g). These cells were used in a nude mouse xenograft model. Tumours were significantly larger in mice injected with control MDA-MB-231 cells; however, little tumour growth was observed in the mice injected with CHIP^OE^ cells (Fig. 2h, i). These results suggest that CHIP suppresses tumour progression.

We next used MCF-7 cells to investigate the roles of CHIP in anchorage-independent cell growth and invasiveness of cancer cells,

both hallmarks of tumour progression. Control cells and sh*CHIP* cells proliferated at similar rates under normal culture conditions (Fig. 3a). sh*CHIP* increased the number of colonies in soft agar (colony-formation assay; Fig. 3b), suggesting that *CHIP* knockdown enhances anchorage-independent cell growth. Next, to examine the invasive and metastatic potential of these cells, we performed migration and invasion assays. In a migration assay, we found that sh*CHIP* increased the ability of cells to migrate (Fig. 3c). We also investigated the invasiveness of these cells (invasion assay), and found that sh*CHIP* significantly increased the number of cells that penetrated the Matrigel-coated membrane (Fig. 3d). The results of these assays indicate that the metastatic potential of the cancer cells was significantly enhanced by *CHIP* knockdown.

We performed a similar set of experiments using sh*CHIP* and CHIP^OE^ MDA-MB-231 cells (Fig. 3e–3h). Changing the CHIP level did not markedly affect cell growth under normal culture conditions (Fig. 3f). However, knockdown increased, whereas overexpression decreased anchorage-independent cell growth (Fig. 3g) and metastatic potential (Fig.3h) of MDA-MB-231 cells. Thus, these results indicate that
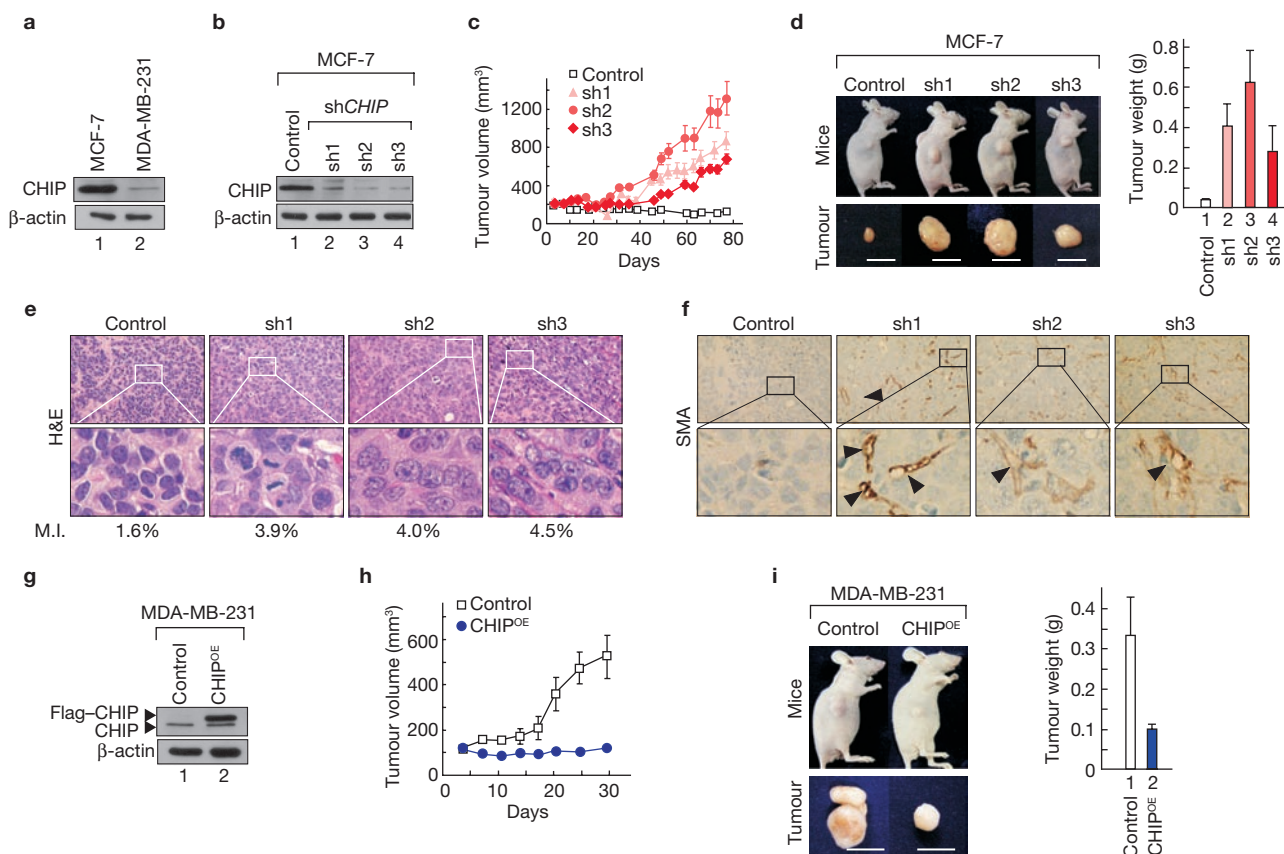
Figure 2 CHIP suppresses tumour growth in a mouse xenograft model. (**a**)
Expression level of CHIP in the MCF-7 or MDA-MB-231 cells. Protein levels
of CHIP in the cells were determined by immunoblotting. (**b**) Knockdown
of *CHIP* using shRNA (sh*CHIP*). Retrovirus was used to infect MCF-7
cells, which were selected with G418 (1 mg ml⁻¹). CHIP protein levels
were assessed by immunoblotting. (**c**) Tumour growth curves in nude mice
inoculated with control or sh*CHIP* MCF-7 cells. Ten nude mice received
bilateral subcutaneous injections of control or sh*CHIP* cells. Tumour volume
is presented as the mean ± s.d. ($n = 20$) from 10 mice in each group. (**d**)
Increased tumour size in mice injected with sh*CHIP* cells. Photographs of
representative nude mice (left, upper panels) and tumours (left, lower panels)
are shown. The scale bars represent 10 mm. Tumour weights after 77 days
are shown on the right. Bars represent mean + s.d. ($n = 20$). (**e**, **f**) *CHIP*
knockdown leads to a higher nuclear grade and increased vascularization of
tumour cells. Sections of tumours from mice injected with control or sh*CHIP*

cells were stained with haematoxylin and eosin (H&E, **e**) or labelled with anti-
SMA antibodies (SMA, **f**). Mitotic index (M. I.) values are shown below the
H&E images. Arrowheads (**f**) indicate SMA-positive vessels. (**g**) Expression of
Flag–CHIP in MDA-MB-231 cells. Plasmid vector containing Flag–CHIP
(CHIP) or empty vector (control) was transfected into MDA-MB-231 cells,
which were selected with G418 (1 mg ml⁻¹). CHIP protein levels in the cells
were analysed by immunoblotting. (**h**) Tumour growth curves in nude mice
inoculated with control or CHIP^OE cells. Nude mice received subcutaneous
injections of control or CHIP^OE cells. Tumour volume is presented as the
mean ± s.d. ($n = 10$). (**i**) Thirty days after the injections, the mice were
killed and tumour tissues were collected. The photographs in the left
panel show representative nude mice (upper) and tumours (lower). The
scale bars represent 10 mm. The graph in right panel shows the weight of
the 10 tumours after 30 days. Bars represent mean + s.d. ($n = 10$). See
Supplementary Information, Fig. S7 for full scans of blots in **a**, **b** and **g**.

the CHIP expression level was inversely correlated with the malignant
phenotype of breast cancer cells, which was characterized by increased
anchorage-independent cell growth and metastatic potential.

In human breast cancer tissues, we did not observe an inverse cor-
relation between CHIP expression and ERα positivity. In addition, in
ERα-negative MDA-MB-231 cells, anchorage-independent cell growth
and metastatic potential were influenced by the CHIP expression level.
These results suggest that CHIP is able to suppress tumour progression
in the absence of ERα, raising the possibility that besides ERα, other
CHIP target proteins may participate in tumour progression.

We then investigated the molecular mechanism by which CHIP pro-
tein suppresses the malignant phenotype. Given that CHIP is a U-box
E3 ubiquitin ligase[1–4], it may act by degrading several proteins that con-
tribute to tumour progression. To test this hypothesis, we compared
the levels of oncogenic proteins in control and sh*CHIP* MCF-7 cells
by immunoblotting (Fig. 3i). The levels of the breast cancer-related

protein SRC-3 (steroid receptor co-activator 3, ref. 13), which is also
known as AIB1 (ref. 14), ACTR[15], TRAM-1 (ref. 16), p/CIP[17] and RAC3
(ref. 18), was upregulated in sh*CHIP* cells. The levels of anti-apoptotic
proteins, such as Bcl2 (refs 20, 21) and Akt1 (ref. 22), were higher in the
sh*CHIP* cells (Fig. 3i), which is related to enhancement of anchorage-
independent cell growth in sh*CHIP* cells (Fig. 3b). Expression levels
of Smad2, a signal transducer in the TGF-β signalling pathway[23,24], as
well as Twist, β-catenin and vimentin, which are marker proteins of the
epithelial–mesenchymal transition (EMT)[25,26], were also upregulated.
TGF-β signalling pathways are known to be related to aggressive phe-
notypes in tumours, including invasion and migration[23,24], and the EMT
allows benign tumour cells to metastasize[26]. Thus, this regulation may
account for the enhanced migration (Fig. 3c) and invasion (Fig. 3d) of
sh*CHIP* MCF-7 cells.

Next, we examined whether the altered protein levels correlated with
changes in the corresponding transcript levels using real-time RT–PCRs
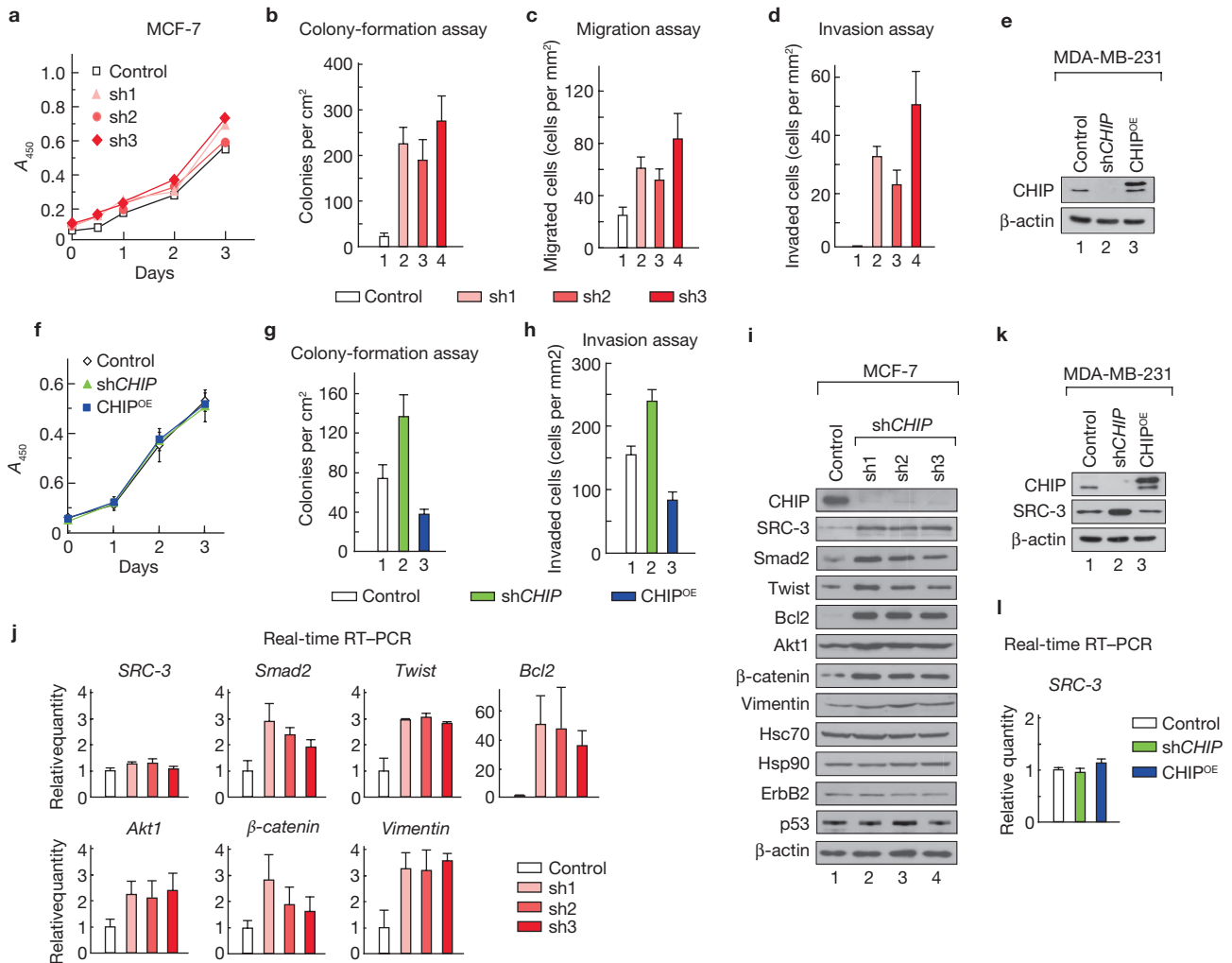
Figure 3 Downregulation of CHIP expression results in the malignant transformation of MCF-7 cells. (**a**) Proliferation of sh*CHIP* MCF-7 cells. Growth rates of control or sh*CHIP* cells were measured by MTT assay. (**b**) Increased anchorage-independent cell growth in sh*CHIP* cells. Cells were plated in soft-agar dishes. After incubation for 3 weeks, colonies were examined under a microscope and colonies with a diameter of more than 100 μm were counted. (**c**, **d**) Enhanced migration and invasion by sh*CHIP*. Control or sh*CHIP* MCF-7 cells were seeded onto filters with an 8-μm pore size in uncoated (**c**, migration assay) or Matrigel matrix-coated (**d**, invasion assay) upper chambers. Both assays were allowed to proceed for 24 h. The average numbers of cells that migrated or invaded per mm^2 are shown. (**e**) Expression level of CHIP in control, sh*CHIP*, or CHIP^{OE} MDA-MB-231 cells. Protein levels of CHIP were determined by immunoblotting. (**f**) Proliferation of the MDA-MB-231 cell lines. Growth rates were measured by MTT assay. (**g**) Inverse correlation between anchorage-independent cell growth and CHIP expression. (**h**) Inverse correlation between invasive activity and CHIP expression. (**i**) Proteins potentially involved in the malignant transformation of sh*CHIP* cells. Total protein levels in sh*CHIP* or control MCF-7 cells were analysed by immunoblotting. (**j**) Genes potentially involved in the malignant transformation of sh*CHIP* cells. Total RNA was isolated from sh*CHIP* or control cells, and gene expression profiles were analysed using real-time RT–PCRs. (**k**) Expression level of SRC-3 in sh*CHIP* or CHIP^{OE} MDA-MB-231 cells. The level of SRC-3 protein was determined by immunoblotting. (**l**) *SRC-3* mRNA expression in the cells. Total RNA was prepared from the cells and the *SRC-3* mRNA level was quantified using real-time RT–PCRs. Data represent mean + s.d., $n = 3$ (**a–d**, **f–h**, **j**, **l**). See Supplementary Information, Fig. S7 for full scans of blots in **e**, **c** and **k**.

(Fig. 3j). The transcript levels of most of the genes, which encode the proteins shown in Fig. 3i, fluctuated in parallel with their protein levels, demonstrating that this regulation occurred at the mRNA level. These results raise the possibility that CHIP regulates transcription factor(s), which in turn regulate the transcription of other oncogenes. Among the candidate CHIP target proteins shown in Fig. 3i, SRC-3 is a strong possibility, because accumulation of SRC-3 protein following *CHIP* knockdown was not due to the accumulation of mRNA (Fig. 3j). In MDA-MB-231 cells, we also observed that the CHIP level affected the level of SRC-3 protein (Fig. 3k), but not its mRNA level (Fig. 3l). Furthermore, SRC-3 is known to be a co-activator of several transcription factors that show elevated expression levels and copy numbers in

human breast and ovarian cancers[13–18]. It has also been reported that levels of SRC-3 are correlated with tumour malignancy[19].

Immunoprecipitation and immunoblot analysis showed that SRC-3 and CHIP interact with each other in cells (Fig. 4a, b). CHIP expression resulted in a decrease in the steady-state levels of SRC-3 protein, an effect that was abolished in the presence of the proteasome inhibitor MG132 (Fig. 4c). Pulse-chase experiments showed that the turnover rate of SRC-3 decreased in sh*CHIP* cells ($t_{1/2} \gg 12$ h) and increased in CHIP^{OE} cells ($t_{1/2} < 4$ h), compared with that in the control cells ($t_{1/2} \approx 8$ h) (Fig. 4d; Supplementary Information, Fig. S5). A ubiquitylation assay revealed that CHIP enhanced the ubiquitylation of SRC-3 (Fig. 4e). Taken together, these results indicate that CHIP mediates the ubiquitylation-dependent
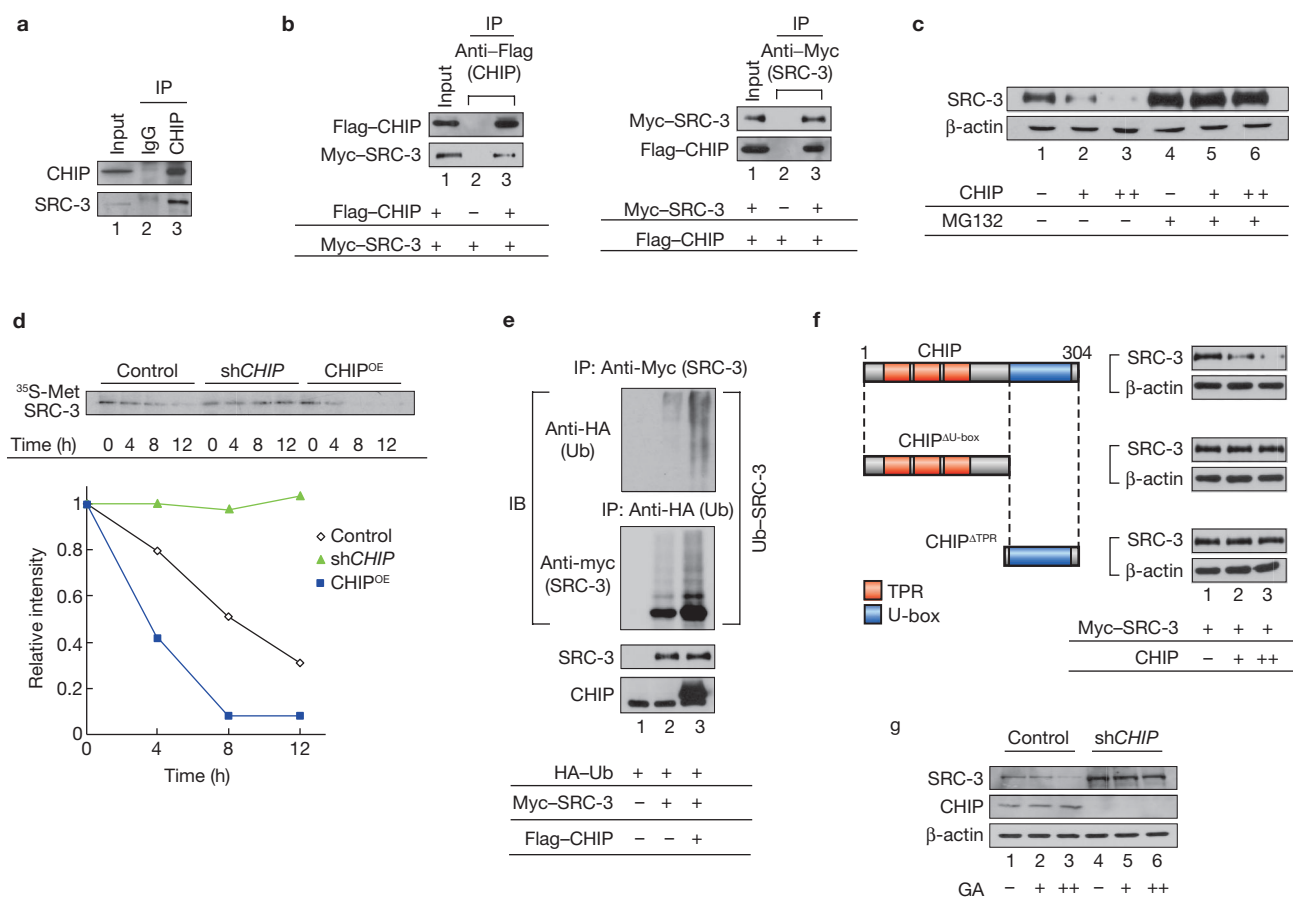
Figure 4 CHIP targets SRC-3 for ubiquitylation and degradation.
(**a**, **b**) CHIP interacts with SRC-3. Cell lysates from MCF-7 cells were immunoprecipitated using control (IgG) or anti-CHIP antibodies, and immunoblotted using the indicated antibodies (**a**). Flag-tagged CHIP and 6× Myc-tagged SRC-3 were expressed in 293 cells with MG132 (10^{-6} M). Cell lysates were immunoprecipitated using anti-Flag (left) or anti-Myc (right) antibodies, and immunoblotted using the indicated antibodies (**b**). (**c**) Reduction of the steady-state SRC-3 protein level due to CHIP expression. A plasmid encoding 6× Myc-tagged SRC-3 (150 ng) was co-transfected into 293 cells with various amounts of plasmid encoding Flag-tagged CHIP (0, 15 or 30 ng). The cells were cultured in the absence or presence of MG132 (1 μM). The level of SRC-3 protein was examined by immunoblotting. (**d**) CHIP facilitates the turnover of SRC-3. Control, shCHIP, or CHIP^{OE} MDA-MB-231 cells were incubated in medium containing ^{35}S-Met, replaced with label-free medium, and collected at the indicated time-points. SRC-3 was immunoprecipitated, subjected to SDS–PAGE, detected on an autoradiograph (upper panel) and the label intensity was quantified

(lower graph). (**e**) Ubiquitylation of SRC-3 is induced by CHIP. HA-tagged ubiquitin was co-expressed in 293 cells with 6× Myc–SRC-3 (lane 2) or 6× Myc–SRC-3 and Flag–CHIP (lane 3) with MG132 (10^{-6} M). 6× Myc-tagged SRC-3 was immunoprecipitated using anti-Myc antibodies. Ubiquitylation was detected using anti-HA antibodies, or ubiquitylated proteins were immunoprecipitated using anti-HA antibodies and ubiquitylated SRC-3 was detected with anti-Myc antibodies (upper panels). SRC-3 or CHIP was detected in whole-cell lysates using anti-Myc or anti-CHIP antibodies, respectively (lower panels). (**f**) The TPR and U-box domains are both required for SRC-3 degradation. Various amounts of plasmid encoding CHIP, CHIP$^{\Delta U}$-box, or CHIP$^{\Delta TPR}$ (0, 15 or 30 ng) were transfected into 293 cells expressing 6× Myc-tagged SRC-3. The levels of SRC-3 protein were examined by immunoblotting. (**g**) Geldanamycin (GA) enhanced CHIP-dependent SRC-3 degradation. Control or shCHIP MDA-MB-231 cells were untreated (lanes 1, 4) or treated with GA (1 μM, lanes 2, 5; 3 μM, lanes 3, 6) for 24 h. SRC-3 protein levels were examined by immunoblotting. See Supplementary Information, Fig. S7 for full scans of blots in **b**–**g**.

degradation of SRC-3. We then created two constructs: CHIP$^{\Delta U}$-box, in which the U-box domain (required for ubiquitylation) was deleted, and CHIP$^{\Delta TPR}$, in which the Hsp-binding TPR domain was deleted[6]. Cells expressing either of the constructs were unable to degrade SRC-3 (Fig. 4f), suggesting that CHIP binds to Hsps to promote the ubiquitylation of their substrate protein, SRC-3. Moreover, SRC-3 protein became unstable when the protein re-folding activity of Hsp90 was inhibited using geldanamycin, consistent with a contribution of Hsps to the CHIP-dependent degradation of SRC-3 (Fig. 4g). SRC-3 is also known to be a target protein of the ubiquitin ligase Fbw7 (ref.27). We found that Fbw7 was not affected by CHIP knockdown in MCF-7 cells (Supplementary Information, Fig. S1a).

Our results raise the possibility that upregulation of SRC-3 protein expression following CHIP knockdown may in turn lead to the altered gene expression shown in Fig. 3i. To test this possibility, we generated MCF-7 cell lines in which expression of SRC-3, CHIP or both CHIP and SRC-3 was suppressed using shRNAs (shSRC-3, shCHIP or shCHIP/shSRC-3). In shCHIP/shSRC-3 cells, the levels of Smad2 and Twist proteins, which were elevated in the shCHIP cells, were reduced to control levels, whereas the level of Akt1 protein was unchanged and that of Bcl2 protein was slightly reduced (Fig. 5a). Similar results were obtained when the expression profiles of these genes were examined (Fig. 5b). IGF-1 has been previously reported to be a target of SRC-3 and to contribute to tumorigenic phenotypes induced by SRC-3 (ref.28). However,
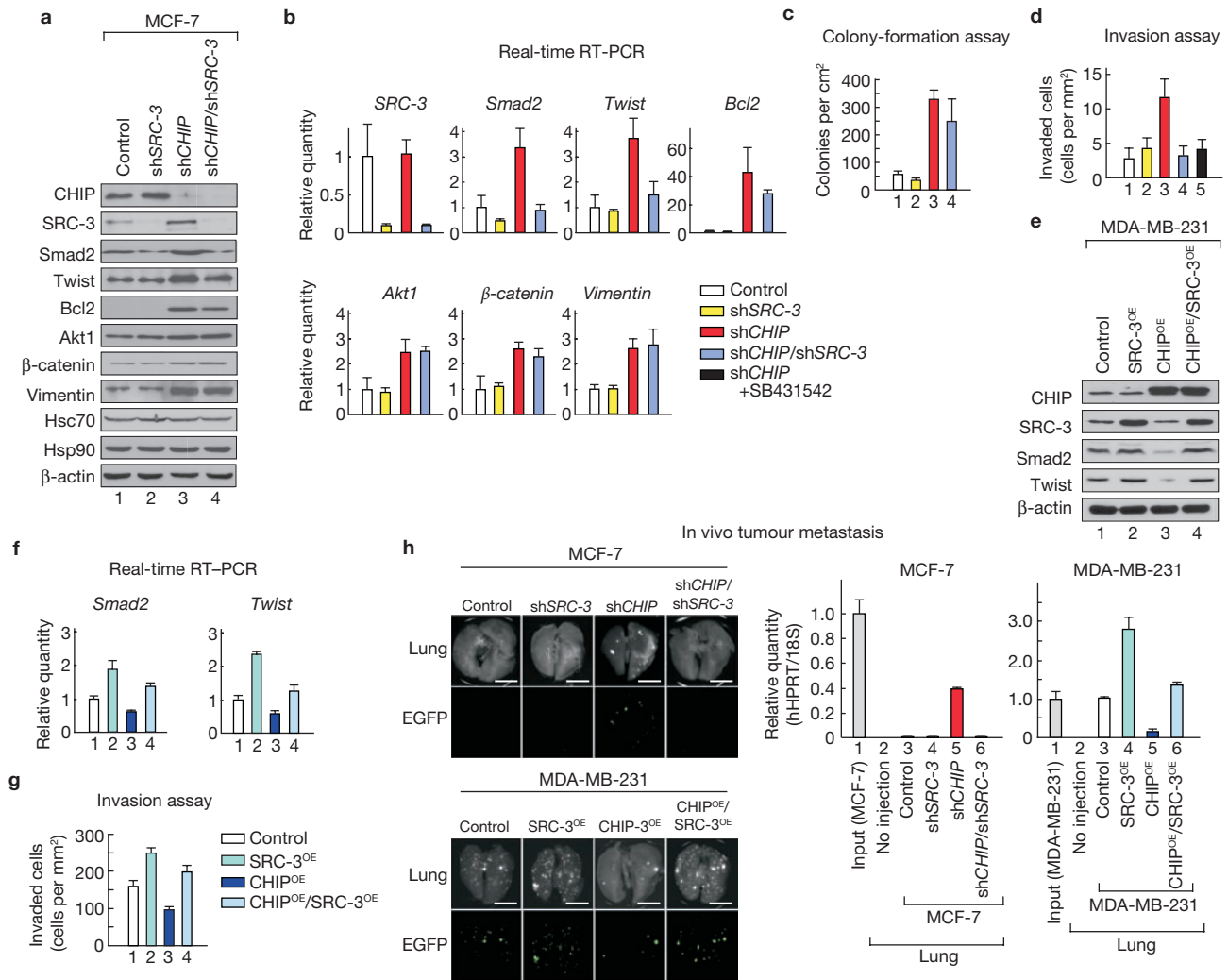
Figure 5 SRC-3 is the downstream regulator of CHIP during cancer metastasis. (**a, b**) Effect of downregulating SRC-3 on protein or transcription levels. Total proteins in the control, sh*SRC-3*, sh*CHIP*, or sh*CHIP*/sh*SRC-3* MCF-7 cells were analysed by immunoblotting (**a**). Total RNA was isolated from the indicated cells, and gene expression profiles were analysed using real-time RT–PCR (**b**). (**c**) A slight decrease in anchorage-independent cell growth following *SRC-3* knockdown. Colony-formation assays were performed as described in Fig. 3b. (**d**) Reduced invasiveness following *SRC-3* knockdown. Invasion assays were performed as described in Fig. 3d. sh*CHIP* cells were treated with the TGF-β inhibitor SB431542 (10 μM; lane 5). The numbers of invasive cells per mm² are shown. (**e, f**) Effect of SRC-3 on protein or transcription levels in MDA-MB-231 cells. Total protein in control, SRC-3^{OE}, CHIP^{OE}, or CHIP^{OE}/SRC-3^{OE} MDA-MB-231 cells were examined by immunoblotting (**e**). Total RNA was prepared from the indicated cells and expression of *Smad2* or *SRC-3* was analysed using real-time RT–PCR (**f**). (**g**) SRC-3 rescues the CHIP^{OE}-induced reduction in invasive activity. Invasive activities of the indicated cell lines were assayed as described in Fig. 3d. (**h**) Effect of SRC-3 on tumour metastasis *in vivo*. EGFP-labelled control, sh*SRC-3*, sh*CHIP* or sh*CHIP*/sh*SRC-3* MCF-7 cells were injected into the tail veins of nude mice ($n = 5$). Alternatively, EGFP-labelled control, SRC-3^{OE}, CHIP^{OE}, or CHIP^{OE}/SRC-3^{OE} MDA-MB-231 cells were injected into the tail veins of nude mice ($n = 5$). Six weeks after the injections, the mice were killed and lung metastasis was detected by fluorescence microscopy (left panel) and quantified by real-time RT–PCR (right graph). Specific primers for human HPRT were used. Scale bars represent 5 mm (left). Data are mean + s.d., $n = 3$ (**b**–**d**, **f**, **g**) and mean + s.d., $n = 5$ (**h**, right). See Supplementary Information, Fig. S7 for full scans of blots in **a** and **e**.

altering SRC-3 expression did not affect the IGF-1 signalling pathway (Supplementary Information, Fig. S1c, d).

We next investigated whether *Smad2* and *Twist* are direct targets of SRC-3. Chromatin immunoprecipitation and transcription assays revealed that *Smad2* is a direct target of SRC-3 (Supplementary Information, Fig. S2). We also showed that Smad2 bound to the promoter region of *Twist*, in agreement with previous reports[29]. These observations demonstrate that SRC-3 increases the level of *Twist* expression by enhancing *Smad2* expression.

We then examined the anchorage-independent cell growth and invasiveness of the sh*CHIP*/sh*SRC-3* MCF-7 cells. Consistent with

the expression profiles of *Bcl2* and *Akt1*, anchorage-independent cell growth was similar in sh*CHIP*/sh*SRC-3* and sh*CHIP* MCF-7 cells (Fig. 5c). In contrast, the invasiveness of sh*CHIP* MCF-7 cells was significantly reduced by *SRC-3* knockdown (sh*CHIP*/sh*SRC-3*; Fig. 5d). Given that the TGF-β/Smad pathway is known to regulate *Twist* transcription and enhance cancer invasion[23,24,29], our results suggest that the enhanced metastatic activity in sh*CHIP* MCF-7 cells was a result of the enhanced Smad2 and Twist expression mediated by SRC-3. This idea was supported by the inhibition of sh*CHIP* cell invasiveness after treatment with the TGF-β inhibitor SB431542 (Fig. 5d). Moreover, in MDA-MB-231 cells, CHIP^{OE} reduced levels of *Smad2*

and *Twist* mRNA and SRC-3 protein. *Smad2* and *Twist* mRNA levels were restored by co-overexpression of SRC-3 with CHIP (CHIP[OE]/SRC-3[OE]) (Fig. 5e, f). As expected, the repression of invasive activity by CHIP[OE] was restored in CHIP[OE]/SRC-3[OE] cells (Fig. 5g).

Finally, to investigate whether *CHIP* knockdown in MCF-7 cells enhanced *in vivo* metastatic activity, we injected control and sh*CHIP* MCF-7 cells into the tail veins of nude mice. Lung metastasis was enhanced in mice given the sh*CHIP* MCF-7 cells (Fig. 5h; Supplementary Information, Fig. S3) but *SRC-3* knockdown (sh*CHIP*/sh*SRC-3*) suppressed this effect. In contrast, CHIP[OE] in MDA-MB-231 cells reduced lung metastasis, which was restored by co-overexpression of SRC-3 (CHIP[OE]/SRC-3[OE]).

Our observations indicate that when CHIP expression is reduced, SRC-3 accumulates, leading to enhanced tumour migration and invasion through increased *Smad2* and *Twist* gene transcription (Supplementary Information, Fig. S4). In agreement with this model, we observed a parallel correlation between tumour grade and the SRC-3 protein level (Supplementary Information, Fig. S6). A recent report showed that when CHIP was exogenously expressed, it induced the degradation of Smad proteins[9]. In our experiment, however, accumulation of Smad following *CHIP* knockdown was due to enhancement of transcription rather than inhibition of degradation. Previous reports indicate that Smad proteins are ubiquitylated by other E3 ubiquitin ligases, such as Smurf and SCF/Roc1 (ref. 3). Therefore, CHIP may make a minor contribution to Smad protein degradation, at least in breast cancer cells.

ERα is one of the targets of ubiquitylation and degradation by CHIP[6]. However, we did not observe an inverse correlation between *CHIP* expression and ERα positivity in human breast cancer tissues. ERα protein levels in breast cancers are determined by both transcription and protein degradation, which may explain why ERα protein levels do not correlate with CHIP expression levels. Moreover, CHIP preferentially ubiquitylates misfolded forms of ERα, and functional ERα protein is not a CHIP target[6], which may also account for lack of the inverse correlation between CHIP expression and ERα positivity. Given that SRC-3 is a co-activator of ERα, however, the CHIP/SRC-3/ERα signalling pathway may also participate in ERα-positive breast cancer progression.

Our results also indicate that CHIP suppresses the expression of other oncogenic proteins that enhance anchorage-independent tumour growth (Supplementary Information, Fig. S4). CHIP is known to be involved in degrading misfolded forms of several oncogenic proteins, including p53 and ErbB2. In breast cancer cell lines, the levels of these proteins were not markedly affected by the CHIP level, although we cannot rule out the possibility that CHIP functions in tumour growth suppression by maintaining the overall quality of these proteins.

METHODS

Expression vectors. DNA fragments encoding full-length and various truncated forms of CHIP were amplified by PCR and subcloned into the pcDNA3 vector containing sequences coding for Flag. Similarly, the SRC-3-full-length cDNA was cloned into the pcDNA3 vector containing 6×Myc sequence.

Cell culture and transfection. MCF-7, MDA-MB-231 and 293 cells were maintained in Dulbecco's modified Eagle's medium (DMEM) supplemented with 10% fetal bovine serum (FBS). The proliferation of cultured cells was measured by MTT assay using an MTT cell count kit (Nakarai Tesque). Transfection was performed with PerFectin transfection reagent (Gene Therapy Systems) or Transfast reagent (Promega).

Co-immunoprecipitation and immunoblotting. Cells were lysed in TNE buffer (10 mM Tris-HCl (pH 7.8), 1% NP-40, 0.15 M NaCl, 1 mM EDTA, 1 µM phenylmethylsulphonyl fluoride (PMSF) and 1 µg ml⁻¹ aprotinin). Extracted proteins were immunoprecipitated with the appropriate antibodies. Bound proteins were separated by SDS–PAGE, transferred onto PVDF membranes (Millipore) and immunoblotted with the appropriate antibodies. The antibodies used in this study were: mouse monoclonal antibodies specific for Flag (1:1000; M2; Sigma), c-Myc (1:2000; Nakarai Tesque), β-catenin (1:1000; BD Biosciences), Bcl2 (1:1000; BD Biosciences), Vimentin (1:1000; Sigma), Hsp90 (1:5000; BD Biosciences), p53 (1:5000; Santa cruz), rat monoclonal antibodies against HA (1:500; Roche) and human CHIP (1:1000; Green Space Biomed, Japan), rabbit monoclonal antibody against Smad3 (1:1000; Cell Signaling), rabbit polyclonal antibodies against Twist (1:1000; Sigma), Akt1 (1:1000; Cell Signaling), Hsc70 (1:3000; Streegen), ErbB2 (1:1000; Cell Signaling), IGF-1 (1:250; Abcam), Fbw7 (1:1000; Invitrogen), IGF-1R (1:500; Cell signaling), phospho-IGF-1R (1:500; Cell Signaling) and goat polyclonal antibodies against SRC-3 (1:500; Santa Cruz) and Smad2 (1:1000; Santa Cruz).

Ubiquitylation assay. 293 cells expressing Myc-tagged SRC-3 and/or Flag-tagged CHIP were lysed with radioimmunoprecipitation buffer (50 mM Tris-HCl (pH 7.5), 150 mM NaCl, 1% Nonidet P-40, 0.5% sodium deoxycholate, and 0.1% SDS) supplemented with complete protease inhibitor mixture (Roche) and placed on ice for 20 min. The extracts were cleared by centrifugation and immunoprecipitation reactions were carried out with anti-Myc agarose beads for 3 h at 4°C. After washing the resin with radioimmunoprecipitation buffer, the bound proteins were immunoblotted with the appropriate antibodies.

Pulse-chase experiments. MCF-7 or MDA-MB-231 cells were incubated with Met- and Cys-free medium (Gibco) for 2 h, replaced with medium containing ³⁵S-Met and incubated for 2 h. Cells were then washed three times with phosphate-buffered saline and incubated with medium supplemented with 1 mM non-radioactive Met and Cys for 0, 4, 8 or 12 h. Cells were collected at the indicated times and SRC-3 was immunoprecipitated from cell lysates using anti-SRC-3 antibody. The precipitated SRC-3 was subjected to SDS–PAGE and detected with an autoradiograph.

RNA interference. For stable RNA interference, we used a retroviral expression system. GP2-293 cells (Clontech) were co-transfected with the p10A1 vector and either pSINsi-hU6 (Takara) or pRETRO-SUPER (OligoEngine) vector containing either the CHIP, SRC-3 or luciferase (control) target sequence. MCF-7 or MDA-MB-231 cells were incubated with the retroviral supernatant in the presence of 8 µg ml⁻¹ polybrene. Twenty-four hours after infection, the viral supernatant was replaced with fresh DMEM containing 10% FBS. The infected cells were selected with 1 mg ml⁻¹ G418 or 1 µg ml⁻¹ puromycin. The target sequences were 5′-gcacgacaagtacatggcgga-3′ for CHIP, 5′-ggtcttacctgcagtggtgaa-3′ for SRC-3 and 5′-gaagctgcgcggtggtgttgt-3′ for luciferase.

Soft agar colony-formation assay. For soft agar assays, 10,000 cells were suspended in DMEM containing 0.35% agar and layered on top of 1 ml of DMEM solidified with 0.6% agar in each well of a 6-well plate. After growing at 37 °C for 2–3 weeks, colonies with a diameter of more than 100 µm were counted. The reported results represent the averages of three independent experiments.

***In vitro* assays of cell migration and invasion.** The invasive potential of the MCF-7 or MDA-MB-231 cells was tested with Matrigel invasion chambers (24-well format, 8-µm pore size; BD Biosciences). Briefly, 150,000 cells suspended in DMEM containing 1% FBS were transferred into an insert chamber. In the lower chamber, DMEM containing 10% FBS served as the source of the chemoattractants. After incubation for 24 h, the cells on the upper surface of the filter were wiped away with a cotton swab. The cells on the lower surface of the filters were fixed with methanol for 10 min, stained with Giemsa for 3 h and counted. For each replicate, cells in five randomly selected fields were counted. Migration assays were performed using the same procedure, except that the insert chambers were not coated with Matrigel and DMEM containing 10% FBS was used for the cell suspensions.

***In vivo* tumour formation assay.** BALB/cAJcl-nu/nu female mice at 5 weeks of age were purchased from CLEA Japan. MDA-MB-231 or MCF-7 cells were cultured as monolayers, trypsinized and resuspended in an equal volume of Matrigel

at 5.0×10^7 or 1.0×10^8 cells per ml, respectively. Female nude mice were given bilateral subcutaneous injections of 5.0×10^6 or 1.0×10^7 (0.1 ml) MDA-MB-231 or MCF-7 cells. The mice were kept in a pathogen-free environment. Tumour growth was monitored twice each week by measuring the tumour size using calipers; tumour volume was determined using the formula V = 1/2 × larger diameter × (smaller diameter)². The mice were killed and the tumour tissues were collected, weighed and fixed with 20% formalin. All animal experiments were in accordance with institutional guidelines.

***In vivo* tumour metastasis assay.** BALB/cAJcl–nu/nu female mice at 5 weeks of age were purchased from CLEA Japan. The mice were injected with 1.5×10^6 MDA-MB-231 or MCF-7 cells which stably expressed EGFP, administered through the tail vein. Lungs were collected on day 42 and analysed by fluorescence microscopy. After analysis, the lungs were snap-frozen for RNA extraction. For metastasis quantification, total mRNA from the lung was extracted and reverse transcribed. Complementary DNA was quantitatively analysed by real-time PCR. Specific primers for human *HPRT* that do not cross-react with its mouse counterpart were designed. 18S ribosomal RNA was used for normalization.

Patients and tissue samples. Twenty-seven breast tumour samples were surgically obtained at the Saitama Cancer Center Hospital (Saitama, Japan) after informed consent was obtained from the patients. The Saitama Cancer Center Ethics Committee approved this study. For RNA extraction, tissues were immediately snap-frozen in liquid nitrogen and stored at –80 °C. The clinico-pathological parameters are summarized in Supplementary Information, Table S1.

Real-time RT–PCR. Tissues and cells were homogenized in 1 ml of isogen and total RNA was extracted according to the manufacturer's instructions (Nippon Gene). cDNA was synthesized from total RNA using RevatraAce reverse transcriptase (Toyobo) and oligonucleotides or Randam primers. Real-time PCR was performed to amplify DNA fragments. Primer sequences can be found in Supplementary Information Methods.

Immunohistochemistry. Formalin-fixed mouse and human tumour tissues were embedded in paraffin and sectioned (5 μm). The paraffinized sections were treated with 0.3% hydrogen peroxidase/methanol and incubated with the monoclonal antibodies in 0.01 M citrate buffer (pH 6.0) followed by incubation with secondary antibodies (peroxidase-labelled EnVision reagent; Dako) for 30 min at room temperature. Samples were developed using either AEC or DAB as substrates (Dako).

Statistical analysis. Data are representative of at least three different experiments. Statistical analysis was performed using *t*-test.

Note: Supplementary Information is available on the Nature Cell Biology website.

1. Esser, C., Alberti, S. & Hohfeld, J. Cooperation of molecular chaperones with the ubiquitin/proteasome system. *Biochim.Biophys. Acta* **1695**, 171–188 (2004).
2. Ballinger, C. A. *et al.* Identification of CHIP, a novel tetratricopeptide repeat-containing protein that interacts with heat shock proteins and negatively regulates chaperone functions. *Mol. Cell. Biol.* **19**, 4535–4545 (1999).
3. Connell, P. *et al.* The co-chaperone CHIP regulates protein triage decisions mediated by heat-shock proteins. *Nature Cell Biol.* **3**, 93–96 (2001).
4. McDonough, H. & Patterson, C. CHIP: a link between the chaperone and proteasome systems. *Cell Stress Chaperones.* **8**, 303–308 (2003).
5. Meacham, G. C., Patterson, C., Zhang, W., Younger, J. M. & Cyr, D. M. The Hsc70 co-chaperone CHIP targets immature CFTR for proteasomal degradation. *Nature Cell Biol.* **3**, 100–105 (2001).
6. Tateishi, Y. *et al.* Ligand-dependent switching of ubiquitin-proteasome pathways for estrogen receptor. *EMBO J.* **23**, 4813–4823 (2004).
7. Xu, W. *et al.* Chaperone-dependent E3 ubiquitin ligase CHIP mediates a degradative pathway for c-ErbB2/Neu. *Proc. Natl Acad. Sci. USA* **99**, 12847–12852 (2002).
8. Esser, C., Scheffner, M. & Hohfeld, J. The chaperone-associated ubiquitin ligase CHIP is able to target p53 for proteasomal degradation. *J. Biol. Chem.* **280**, 27443–27448 (2005).
9. Xin, H. *et al.* CHIP controls the sensitivity of transforming growth factor-β signaling by modulating the basal level of Smad3 through ubiquitin-mediated degradation. *J. Biol. Chem.* **280**, 20842–20850 (2005).
10. Kamynina, E., Kauppinen, K., Duan, F., Muakkassa, N. & Manor, D. Regulation of proto-oncogenic dbl by chaperone-controlled, ubiquitin-mediated degradation. *Mol. Cell. Biol.* **27**, 1809–1822 (2007).
11. Fan, M., Park, A. & Nephew, K. P. CHIP (carboxyl terminus of Hsc70-interacting protein) promotes basal and geldanamycin-induced degradation of estrogen receptor-α. *Mol. Endocrinol.* **19**, 2901–2914 (2005).
12. Tateishi, Y. *et al.* Turning off estrogen receptor β-mediated transcription requires estrogen-dependent receptor proteolysis. *Mol. Cell. Biol.* **26**, 7966–7976 (2006).
13. Wu, R. C. *et al.* Selective phosphorylations of the SRC-3/AIB1 coactivator integrate genomic reponses to multiple cellular signaling pathways. *Mol Cell* **15**, 937–949 (2004).
14. Anzick, S. L. *et al.* AIB1, a steroid receptor coactivator amplified in breast and ovarian cancer. *Science* **277**, 965–968 (1997).
15. Chen, H. *et al.* Nuclear receptor coactivator ACTR is a novel histone acetyltransferase and forms a multimeric activation complex with P/CAF and CBP/p300. *Cell* **90**, 569–580 (1997).
16. Takeshita, A., Cardona, G. R., Koibuchi, N., Suen, C. S. & Chin, W. W. TRAM-1, A novel 160-kDa thyroid hormone receptor activator molecule, exhibits distinct properties from steroid receptor coactivator-1. *J. Biol. Chem.* **272**, 27629–27634 (1997).
17. Torchia, J. *et al.* The transcriptional co-activator p/CIP binds CBP and mediates nuclear-receptor function. *Nature* **387**, 677–684 (1997).
18. Li, H., Gomes, P. J. & Chen, J. D. RAC3, a steroid/nuclear receptor-associated coactivator that is related to SRC-1 and TIF2. *Proc. Natl Acad. Sci. USA* **94**, 8479–8484 (1997).
19. Hudelist, G. *et al.* Expression of sex steroid receptors and their co-factors in normal and malignant breast tissue: AIB1 is a carcinoma-specific co-activator. *Breast Cancer Res. Treatment* **78**, 193–204 (2003).
20. Cory, S. & Adams, J. M. The Bcl2 family: regulators of the cellular life-or-death switch. *Nature Rev. Cancer* **2**, 647–656 (2002).
21. Adams, J. M. & Cory, S. The Bcl-2 protein family: arbiters of cell survival. *Science* **281**, 1322–1326 (1998).
22. Manning, B. D. & Cantley, L. C. AKT/PKB signaling: navigating downstream. *Cell* **129**, 1261–1274 (2007).
23. Derynck, R., Akhurst, R. J. & Balmain, A. TGF-β signaling in tumor suppression and cancer progression. *Nature Genet.* **29**, 117–129 (2001).
24. Attisano, L. & Wrana, J. L. Signal transduction by the TGF-β superfamily. *Science* **296**, 1646–1647 (2002).
25. Yang, J. *et al.* Twist, a master regulator of morphogenesis, plays an essential role in tumor metastasis. *Cell* **117**, 927–939 (2004).
26. Lee, J. M., Dedhar, S., Kalluri, R. & Thompson, E. W. The epithelial-mesenchymal transition: new insights in signaling, development, and disease. *J. Cell Biol.* **172**, 973–981 (2006).
27. Wu, R. C., Feng, Q., Lonard, D. M. & O'Malley, B. W. SRC-3 co-activator functional lifetime is regulated by a phospho-dependent ubiquitin time clock. *Cell* **129**, 1125–1140 (2007).
28. Kuang, S. Q. *et al.* AIB1/SRC-3 deficiency affects insulin-like growth factor I signaling pathway and suppresses v-Ha-ras-induced breast cancer initiation and progression in mice. *Cancer Res.* **64**, 1875–1885 (2004).
29. Thuault, S. *et al.* Transforming growth factor-β employs HMGA2 to elicit epithelial-mesenchymal transition. *J. Cell Biol.* **174**, 175–183 (2006).
30. Izzi, L. & Attisano, L. Regulation of the TGFβ signalling pathway by ubiquitin-mediated degradation. *Oncogene* **23**, 2071–2078 (2004).

nature cell biology

DOI: 10.1038/ncb1839
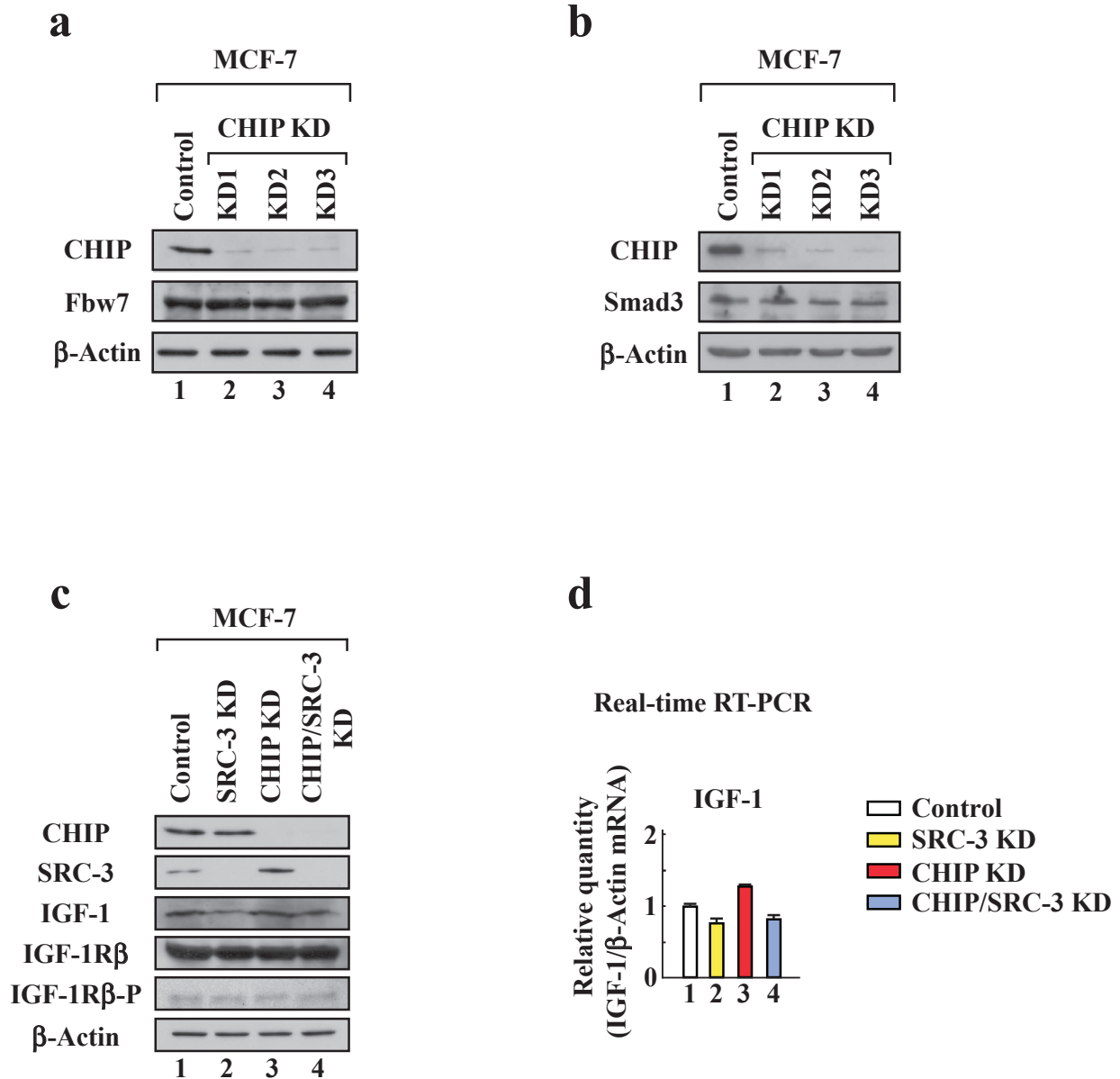
Figure S1 Effect of CHIP KD on the indicated protein and mRNA expression. The level of Fbw7 protein in the CHIP KD or control MCF-7 cells was analyzed by immunoblotting with anti-Fbw7 antibodies. (**b**) Protein level of Smad3 in the CHIP KD or control MCF-7 cells was analyzed by immunoblotting using anti-Smad3 antibodies. (**c**) Level of IGF-1 signaling factors in control, SRC-3 KD, CHIP KD and CHIP/SRC-3 KD MCF-7 cells. Total protein levels in the cells were analyzed by immunoblotting using the indicated antibodies. (**d**) IGF-1 mRNA expression in the cells. Total RNA was prepared from the cells and the IGF-1 mRNA level was quantified using real-time RT-PCRs. Bars represent mean + s.d. (n = 3).

a

b
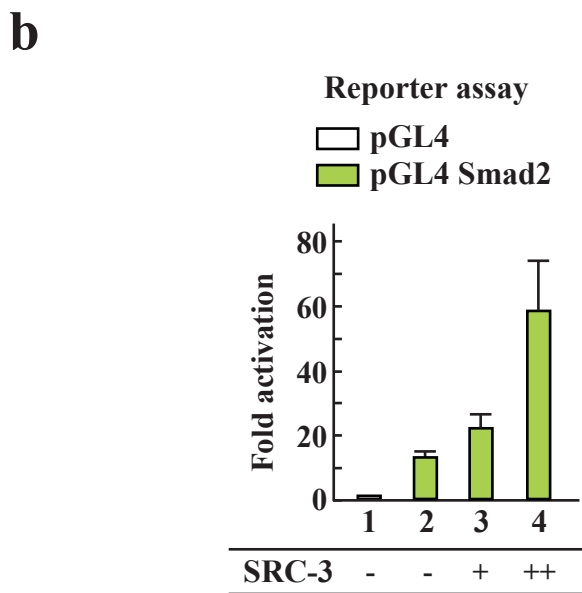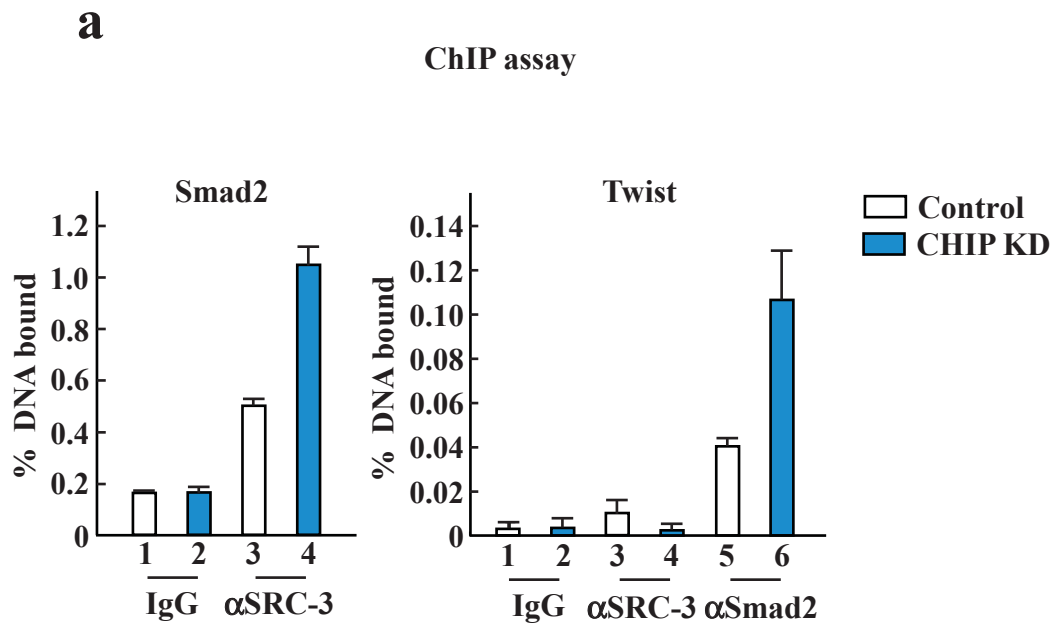
Figure S2 (**a**) Direct binding of SRC-3 to the upstream region of the Smad2 gene. Chromatin immunoprecipitation analysis was performed to examine the binding of SRC-3 or Smad2 proteins to the upstream regions of the Smad2 (-1040 to -937; left graph) and Twist (-130 to -20; right graph) genes in both control and CHIP KD cells. Bars represent mean + s.d. (n = 3). (b) SRC-3 mediated enhancement of transcription from the Smad2 gene promoter by SRC-3. MCF-7 cells were co-transfected with various amounts of SRC-3 expression plasmid and either a luciferase reporter plasmid (pGL4) or a plasmid containing the upstream region of the Smad2 gene (pGL4 Smad2; -1500 to +34). Cell extracts were analyzed using a luciferase assay. Bars represent mean + s.d. (n = 3).

MCF-7

	Control	SRC-3 KD	CHIP KD	CHIP/SRC-3 KD

Mice Lung

EGFP

MDA-MB-231

	Control	SRC-3 OE	CHIP OE	CHIP/SRC-3 OE

Mice Lung
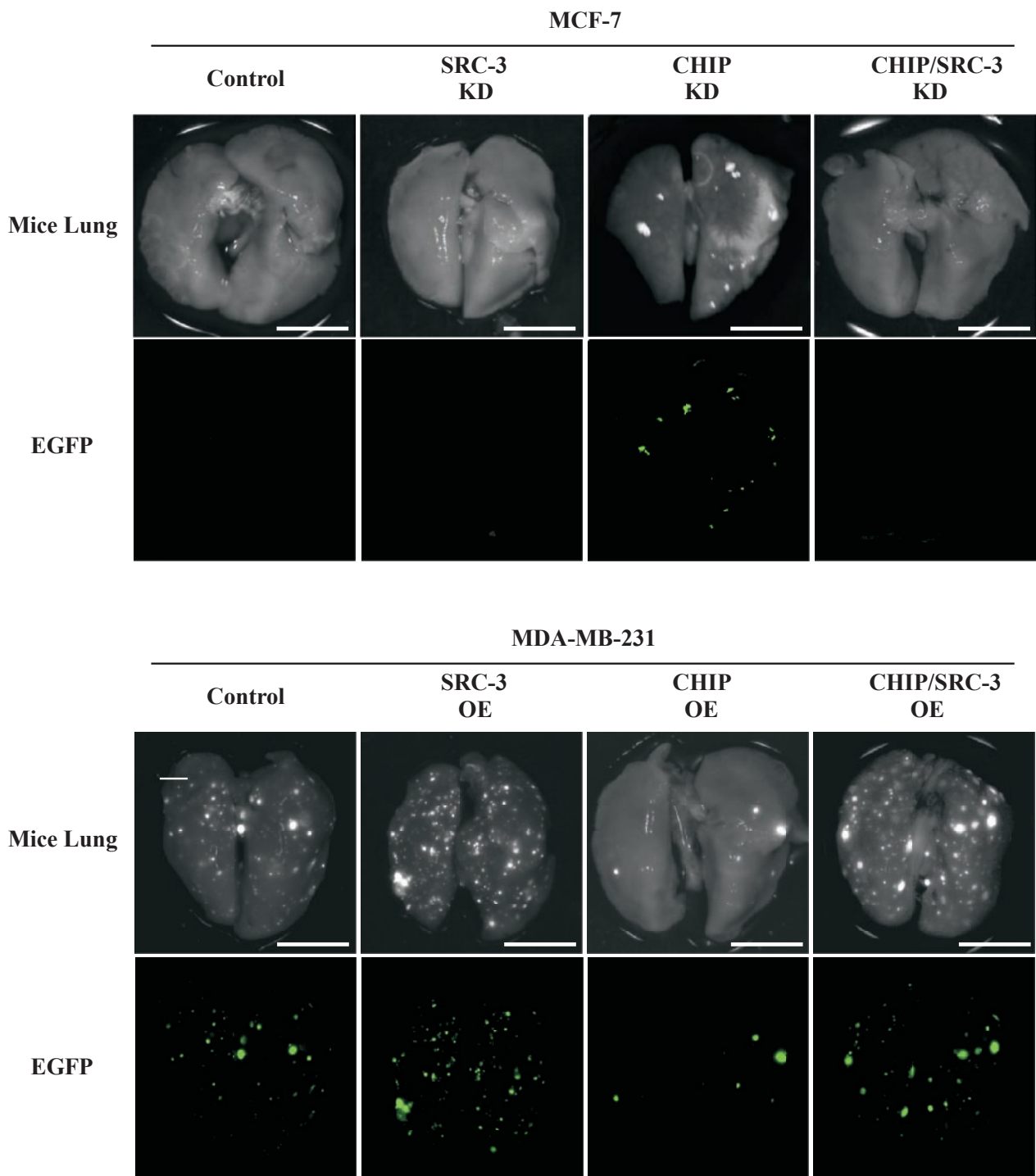
EGFP

Figure S3 Enlarged images of Fig. 5h. EGFP labeled control, SRC-3 KD, CHIP KD, or CHIP/SRC-3 KD MCF-7 cells were injected into tail vain of nude mice. Alternatively, EGFP labeled control, SRC-3 OE, CHIP OE, or CHIP/SRC-3 OE MDA-MB-231 cells were injected into tail vain of nude mice. Six weeks after the injections, the mice were sacrificed, and the lung metastasis was analysed by fluorescence microscopy. Scale bar = 5 mm
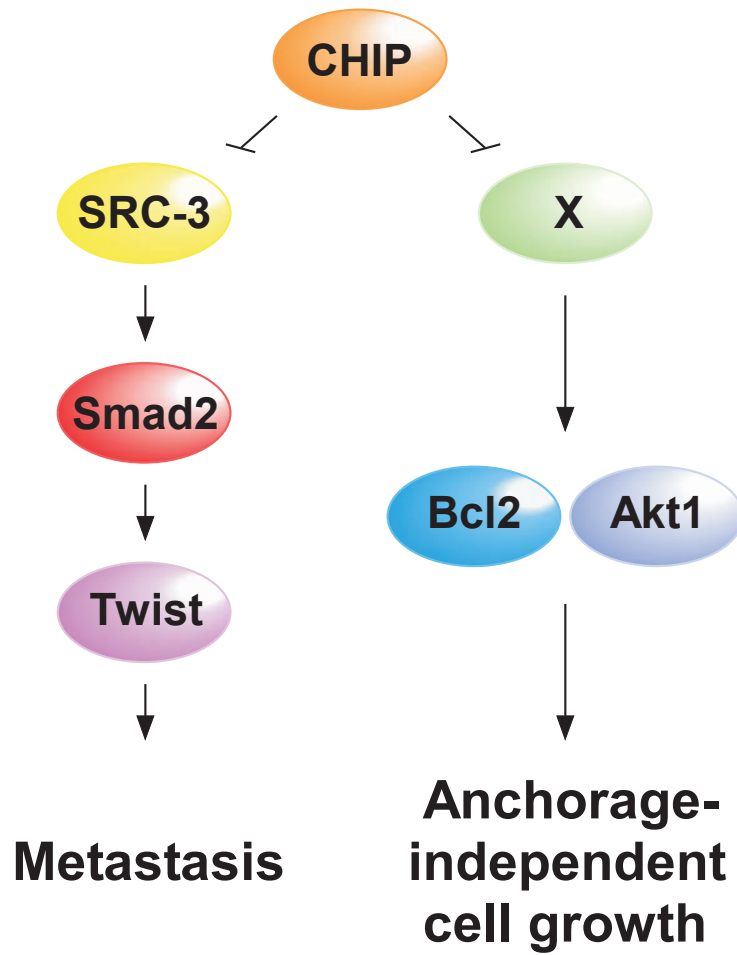
Figure S4 A model for the functions of CHIP in suppression of breast cancer progression.

a

SRC-3

Relative quantity
SRC-3/β-Actin protein

MCF-7   MDA-MB-231

SRC-3

1.00   0.58

β-Actin

1   2

b   Real-time RT-PCR

SRC-3

Relative quantity
SRC-3/β-Actin mRNA

MCF-7   MDA-MB-231

1   2

c

³⁵S Met
SRC-3

MCF-7   MDA-MB-231

Time (h) 0 4 8 12   0 4 8 12

Relative intensity

◆ MCF-7
■ MDA-MB-231

Time (h)
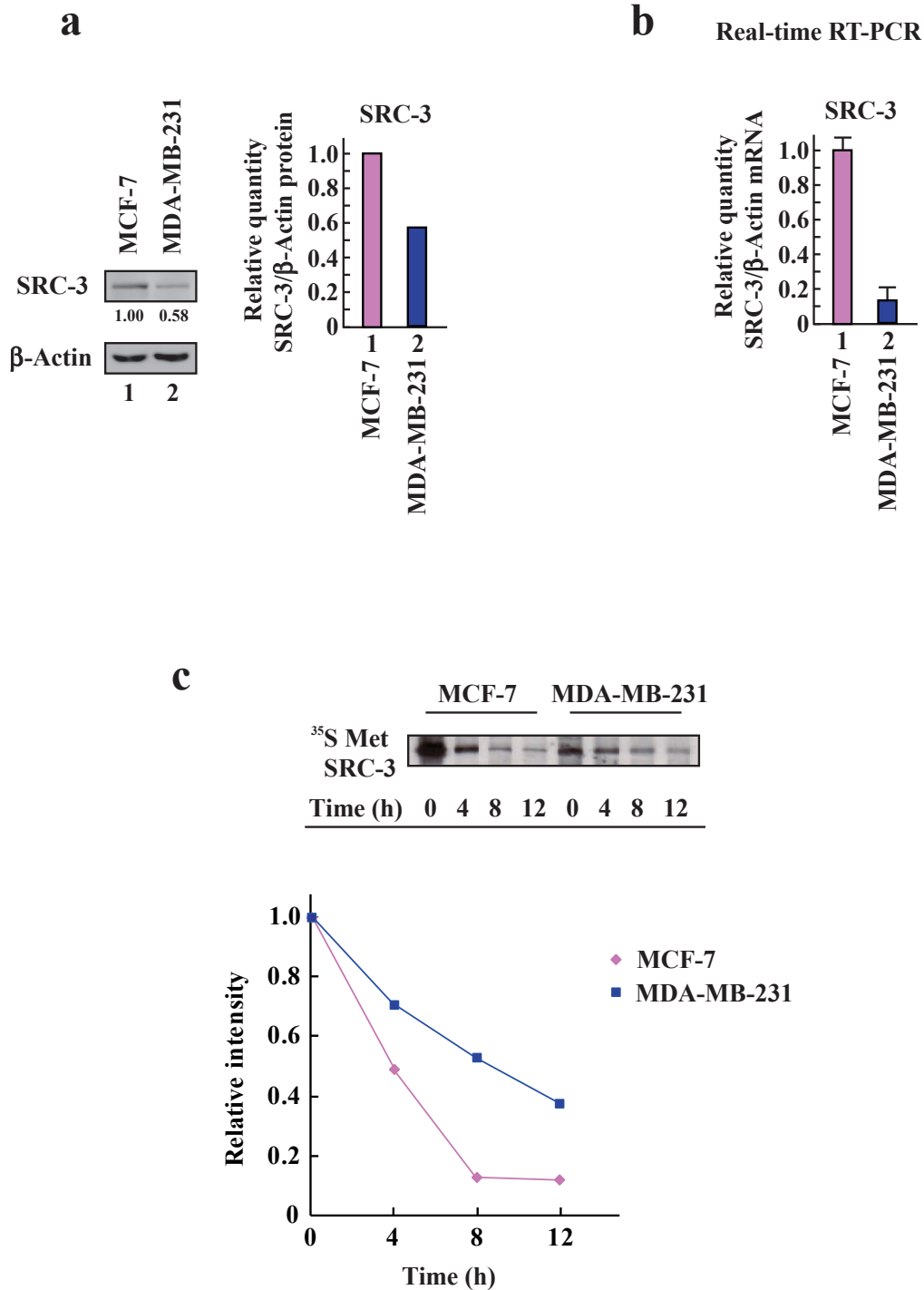
Figure S5 (a) SRC-3 protein level in MCF-7 and MDA-MB-231 cells. The level of SRC-3 protein in MCF-7 or MDA-MB-231 cells was analysed by immunoblotting with anti-SRC-3 antibody. (b) SRC-3 mRNA level in MCF-7 and MDA-MB-231 cells. The level of SRC-3 mRNA in MCF-7 or MDA-MB-231 cells was analysed by real-time RT-PCR. Bars represent mean + s.d. (n = 3). (c) Turnover rate of SRC-3 protein in MCF-7 and MDA-MB-231 cells. SRC-3 protein turnover in MCF-7 and MDA-MB-231 cells were analysed by 35S labeling chase.
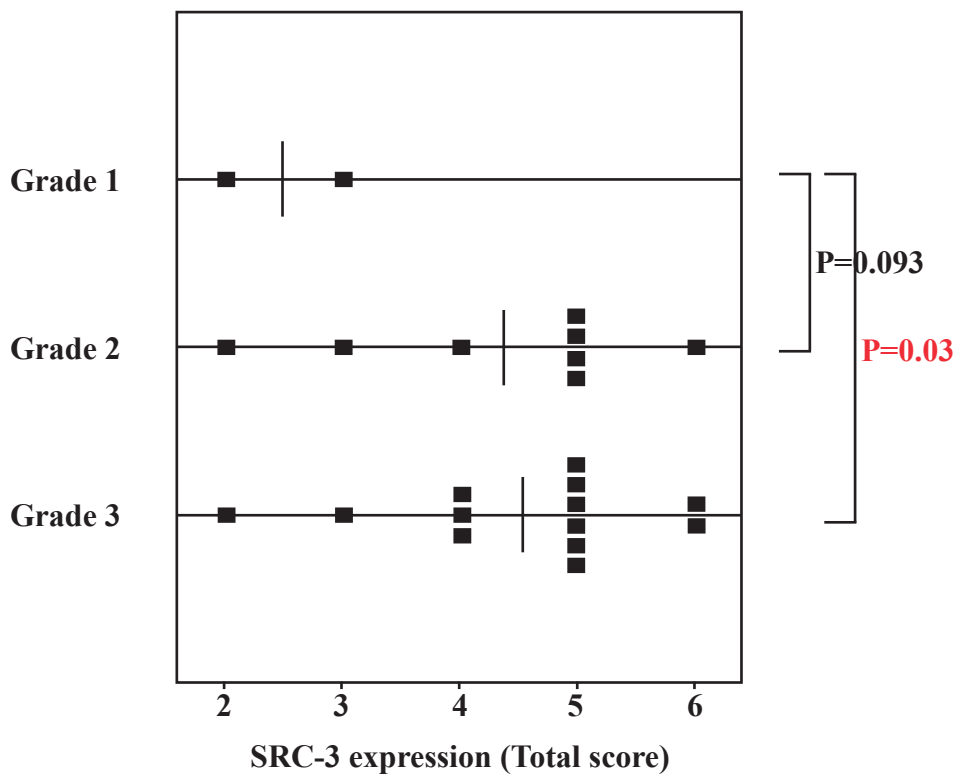
Figure S6 Positive correlation between SRC-3 protein level and histological grade. The level of SRC-3 protein in human breast tumor tissues was analysed by immunostaining with anti-SRC-3 antibody (Becton, Dickinson and Company; BD 611105).
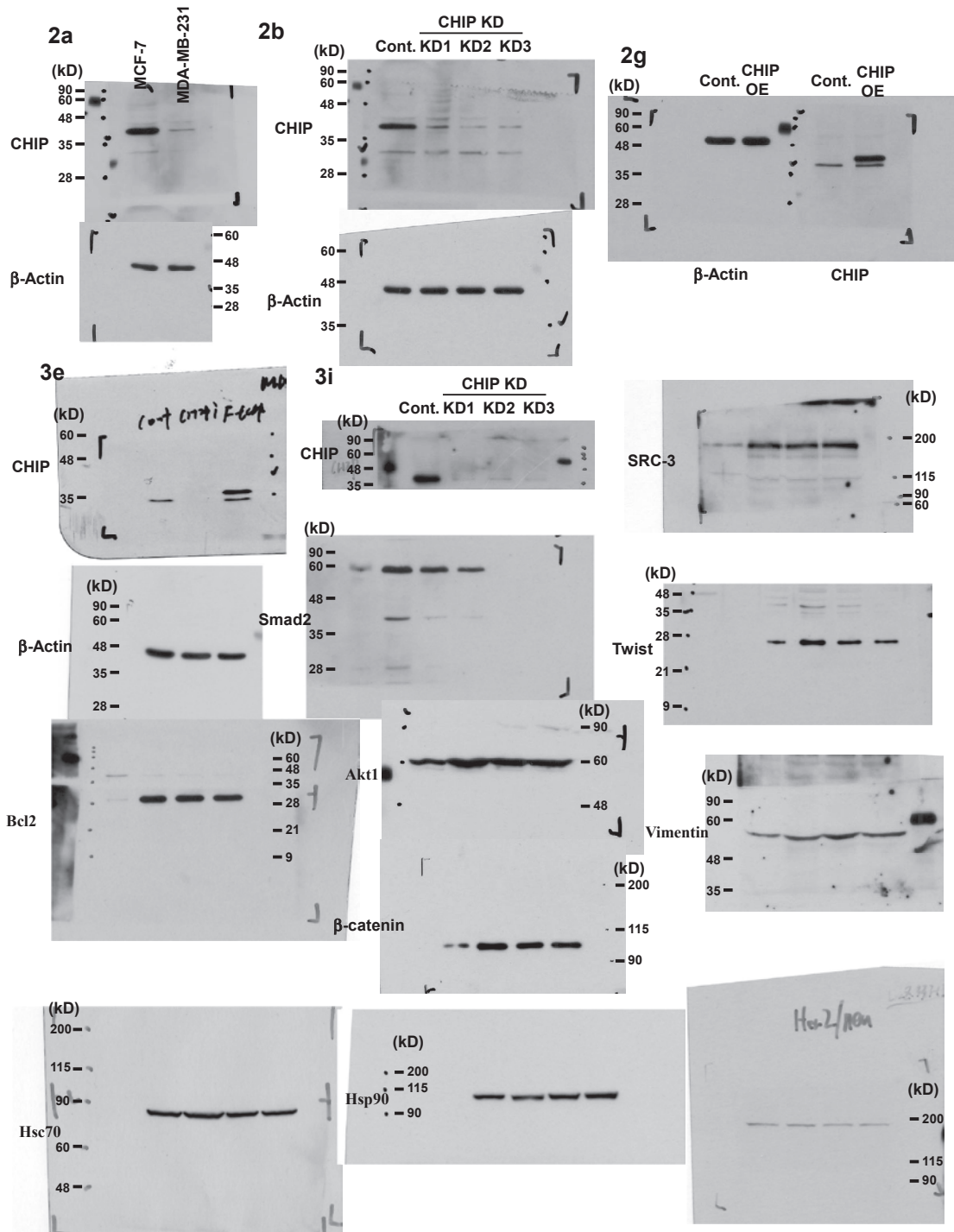
Figure S7 Full blots/scans of original Western data shown in the regular Figures 2a, 2b, 2g, 3e, 3i, 3k, 4a, 4b, 4c, 4d, 4e, 4f, 4g, 5a, and 5e.

Figure S7 continued

4f

4g

5a
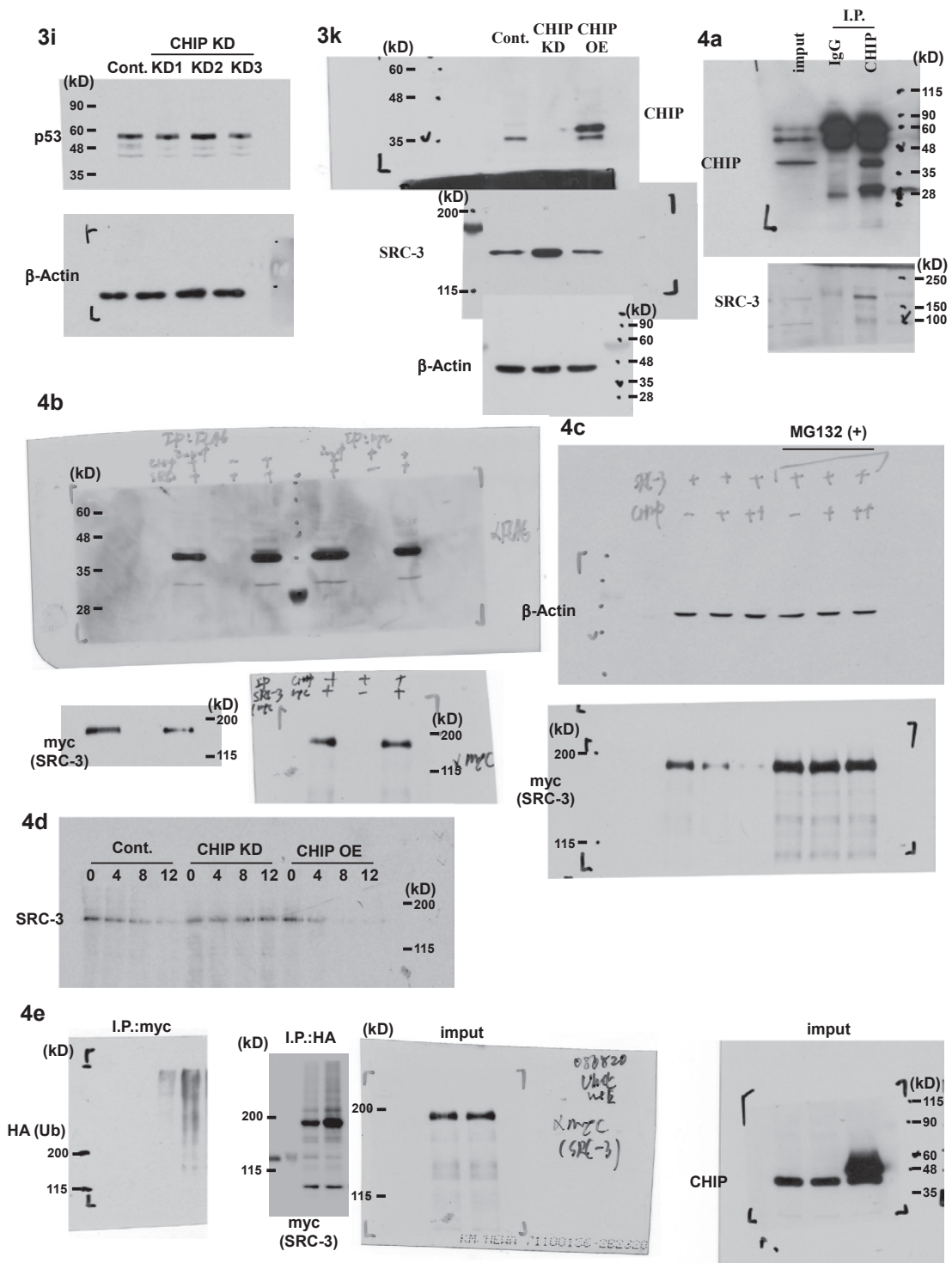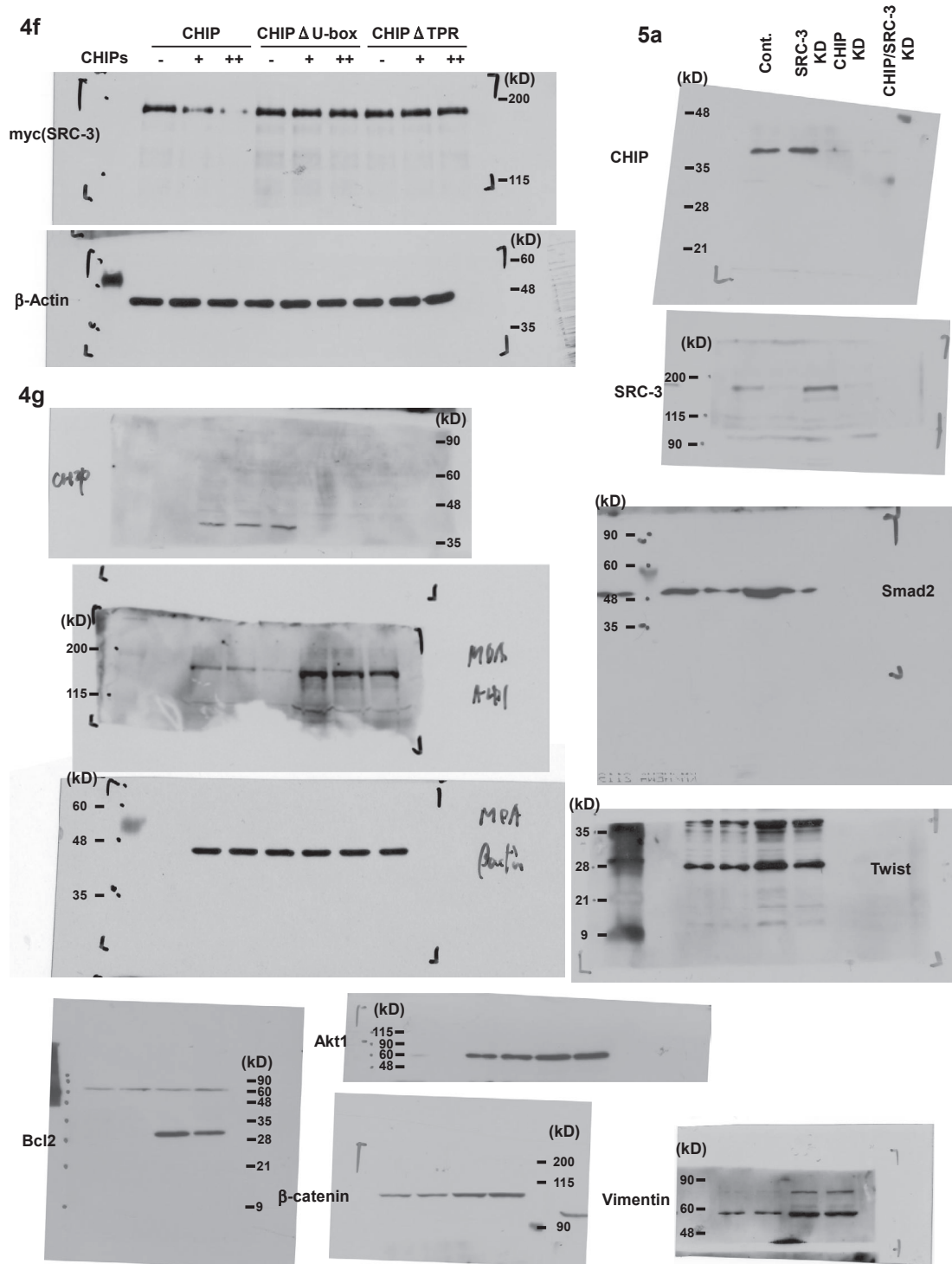
Figure S7 continued

5a

5e
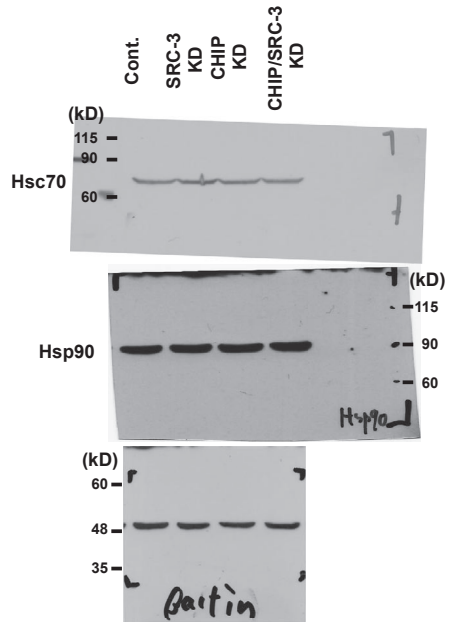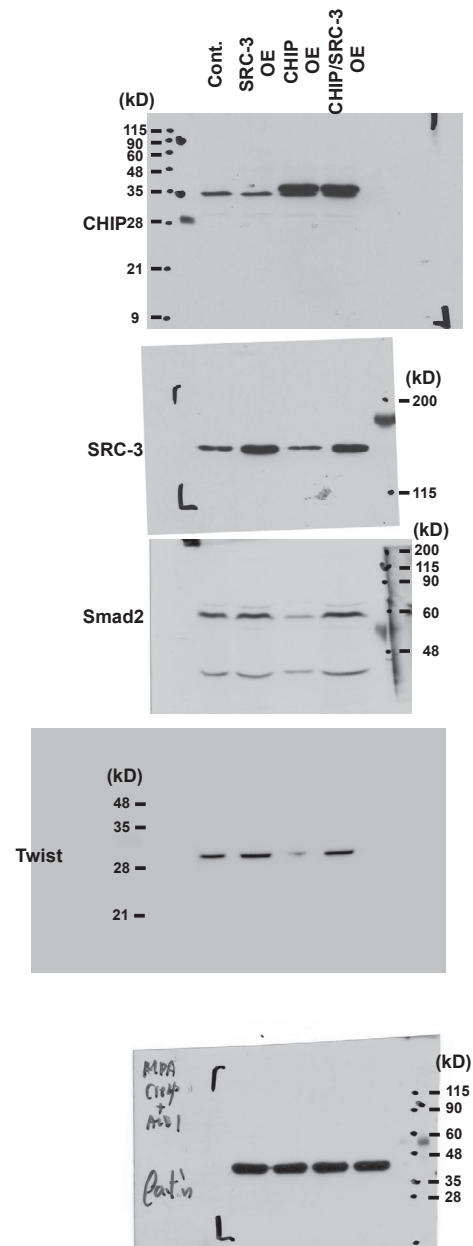
Figure S7 continued

Table S1. Clinicopathological parameters of the breast tumors

		Total No.
Age (yr)	$\leqq$ 50	6
	> 50	21
Menopausal status	Pre	11
	Post	16
Tumor diameter	$\leqq$ 2 cm	15
	> 2 cm	12
ER[a]	Positive	19
	Negative	7
	Unknown	1
PgR[a]	Positive	22
	Negative	4
	Unknown	1
Stage[b]	I	12
	II	14
	III	1
Histology	Invasive ductal	23
	Special	4
Histological grade	1	2
	2	8
	3	13
	Unknown	4
Nodal status[b]	Negative	16
	Positive	11

[a] Cases were considered positive for ER or PgR expression when nuclear staining was observed in at least 10% of the examined tumor cells tested.

[b]Stage and nodal status were determined according to the TMN classifications. Nodal status was interpreted as positive when n score was one or more.

Supplementary Information Methods

Chromatin immunoprecipitation and real-time PCR detection.

Formaldehyde was added to culture medium to a final concentration of 1% to cross-linked nuclear proteins with genomic DNA. After centrifugation, the cell pellets were resuspended in lysis buffer [1% SDS, 10 mM EDTA, protease inhibitors and 50 mM Tris–HCl (pH 8.1)], and sonicated. The lysates were diluted 1:10 in ChIP dilution buffer [0.01% SDS, 1.1% Triton X-100, 1.2 mM EDTA, 16.7 mM NaCl, protease inhibitors and 16.7 mM Tris–HCl (pH 8.1)], and incubated with indicated antibodies overnight at 4°C with rotation. The immuno-complexes were collected with 30 µl of protein G agarose beads (Upstate Biotechnology) for 1 hours at 4°C with rotation. The beads were washed with the following buffers: low salt wash buffer [0.1% SDS, 1% Triton X-100, 2 mM EDTA, 150 mM NaCl and 20 mM Tris–HCl (pH 8.1)], high salt wash buffer [0.1% SDS, 1% Triton X-100, 2 mM EDTA, 500 mM NaCl and 20 mM Tris–HCl (pH 8.1)] and LiCl wash buffer [0.25 mM LiCl, 1% Nonidet P-40, 1% sodium deoxycholate, 1 mM EDTA and 10 mM Tris–HCl (pH 8.1)]. Finally, the beads were washed twice with 1 ml TE buffer [1 mM EDTA and 10 mM Tris–HCl (pH 8.0)]. The immuno-complexes were then eluted by adding 150 µl elution buffer (10mM DTT, 1%SDS, 100mM NaHCO3). The elute was collected and the cross-linking was reversed by adding NaCl to final concentration of 200 mM and incubating overnight at 65°C. The remaining proteins were digested by adding proteinase K. The DNA was phenol precipitated, ethanol precipitated, and amplified by realtime PCR using the Thermal Cycler Dice™ TP800 (Takara) and Platinum SYBR Green qPCR SuperMix-UDG (Invitrogen). The primers for real-time PCR are as follows: 5'-CCTCCTGTAGGGCAGATGTG-3' and 5'-tAatccatgtcccgaagggtc-3' for Smad2

gene upstream resion (-1040 bp to -937 bp), 5'-GGTTTGGGAGGACGAATTGTTAG-3' and 5'-CGTGCAGGCGGAAAGTTTGG-3' for Twist gene upstream resion (-130 bp to -20 bp).

Luciferase reporter assay.

DNA fragments encoding Smad2 gene upstream region (-1500 bp to +13 bp) was amplified by PCR from MCF-7 genome and cloned into a pGL4 reporter plasmid (Promega). For luciferase assays, MCF-7 cells were co-transfected with a pGL4 empty plasmid or a pGL4 containing the upstream region of Smad2 plasmid and pcDNA3 SRC-3 expression plasmid. pRL-CMV, a reference plasmid used to normalize transfection efficiency. Twenty-four hours later, the cells were harvested and cell extracts were prepared. Luciferase assays were performed according to the manufacturer's protocol (Promega). Individual transfections, each of which was performed in three wells, were repeated at least three times. The primers for Smad2 upstream region cloning are as follows: 5'-CTGAAGGCACCCTCCTCTGGGA-3' and 5'-TGCTGGCTGGCGAGCTGCTTCT-3'

Primer sequences for real-time RT-PCR.

β-Actin fw primer: 5'-atcgtccaccgcaaatgcttcta -3'

β-Actin rv primer: 5'-agccatgccaatctcatcttgtt -3'

CHIP fw primer: 5'-aggccaagcacgacaagtacat-3'

CHIP rv primer: 5'-ctgatcttgccacacaggtagt-3'

SRC-3 fw primer: 5'-cagtgattcacgaaaacgca-3'

SRC-3 rv primer: 5'-cagctcagccaattcttcaat-3'

Smad2 fw primer: 5'-accgaaggcagacggtaacaag-3'

Smad2 rv primer: 5'- atgacatgcttgagcaacgcac-3'

β-catenin fw primer: 5'-gaaacggctttcagttgagctg-3'

β-catenin rv primer: 5'-taggatcatcctggcgatatcc-3'

Twist fw primer: 5'-tgcagctatgtggctcacgag-3'

Twist rv primer: 5'-aatgacatctaggtctccggcc-3'

Bcl2 fw primer: 5'-agcatggctcaaagtgcagct-3'

Bcl2 rv primer: 5'-cagatgtccctaccaaccaga-3'

Akt1 fw primer: 5'-aagcaccgcgtgaccatgaac-3'

Akt1 rv primer: 5'-cttggccacgatgacttccttc-3'

Vimentin fw primer: 5'-ggaacgccagatgcgtgaaatg-3'

Vimentin rv primer: 5'-caggtcttggtattcacgaagg-3'.

IGF-1 fw primer: 5'-cctcctcgcatctcttctacctg-3'

IGF-1 rv primer: 5'- ctgctggagccataccctgtg-3'.

HPRT fw primer: 5'-ttccttggtcaggcagtataatcc-3'

HPRT rv primer: 5'-agtctggcttatatccaacacttcg-3'.

18S fw primer: 5'-cgacgacccattcgaacgtct -3'

18S rv primer: 5'-ctctccggaatcgaaccctga -3'.